NANO LETTERS

2008
Vol. 8, No. 6
1667-1672

From Nanorings to Nanodots by Patterning with Block Copolymers

Soojin Park, Jia-Yu Wang, Bokyung Kim, and Thomas P. Russell*

Department of Polymer Science and Engineering, University of Massachusetts, Amherst, Massachusetts 01003

Received February 20, 2008; Revised Manuscript Received April 2, 2008

ABSTRACT

We demonstrate three different transfer patterns that can be achieved by use of a surface reconstructed block copolymer film where metal is evaporated onto the surface of the film, providing the contrast. Thin films of diblock copolymers having cylindrical microdomains oriented normal to the surface with long-range lateral order were used. Solvent reconstruction of the film, followed by a glancing angle metal evaporation and thermal annealing, led to three different decorations of the films with gold. These films were used as masks for pattern transfer of pores, columns, and rings to underlying substrate with high fidelity.

Microphase separated block copolymers (BCPs) offer unique opportunities to control the spatial distribution of nanoparticles, opening pathways to improve the mechanical strength, conductivity, permeability, catalytic activity, and optical and magnetic properties of thin films.[1–5] The ability to control the orientation and lateral ordering of BCP morphologies makes BCP's particularly attractive as scaffolds and templates for the fabrication of nanostructured materials.[6–9] Several methods for incorporating inorganic nanoparticles into polymeric nanostructures have been described. In one, nanoparticles are generated within block copolymer micelles, where metal nanoparticles can be produced by simple chemical methods.[10–12] In another, the cooperative self-organization of nanoparticles and BCPs is used with the need of subsequent chemistry.[9,13–18]

The surface reconstruction of BCPs, as reported previously, is another method to this end.[19–21] Surface reconstruction is a process where, in the case of a diblock copolymer with cylindrical microdomains oriented normal to the surface, upon exposure of the BCP film to a solvent that preferentially dissolves the minor component block, the minor component is drawn to the surface of the film and, upon drying, cylindrical nanopores are produced with dimensions comparable to the original cylindrical microdomains. The minor component block fully coats the surface of the nanoporous film and, as shown by grazing incidence X-ray scattering, if the film thickness is a period of the BCP or less, the nanopores were found to span the film and had vertical side walls. Because the solvent does not alter the chemical structure of the BCP, the reconstruction is fully reversible. So, by heating the film to near its glass-transition temperature, T_g, a full recovery of the initial thin film morphology occurs. However, if the BCP film is heated to temperatures well in excess of T_g, then interfacial interactions will control the orientation of the microdmains. If, prior to heating, metal is evaporated at a glancing angle onto the surface of the reconstructed film, a porous metal film is obtained. If the metal film is thin enough, metal can be drawn into the film. In most pattern transfer approaches, a nanoporous polymer template has been used to transfer a pattern into underlying substrates using RIE and/or milling,[22–26] while the control of spatial location of metal on polymer template can be used as etching masks for preparation of various kinds of nanostructured patterns.

Here we demonstrate three different patterns that can be obtained from the reconstructed BCP film coated with a thin layer of metal. Thin films of polystyrene-*b*-poly(4-vinylpyridine) (PS-*b*-P4VP) BCPs having cylindrical microdomains oriented normal to the surface were used. Reconstruction with ethanol, followed by a glancing angle gold evaporation on the surface and thermal annealing, led three different gold masks or templates that were suitable for pattern transfer into silicon substrates using RIE (SF_6) or as templates for metal evaporation. A pattern of nanoscopic chromium rings, prepared using gold decorated template, is shown.

BCP films were prepared by spin-coating 0.5 wt % PS-*b*-P4VP copolymer toluene/tetrahydrofuran (THF) solutions onto silicon wafers. The copolymer used in the experiments was a PS-*b*-P4VP diblock (Polymer Source) with a molecular weight of 68.7 kg/mol (M_n^{PS} = 47.6 kg/mol; M_n^{P4VP} = 20.9 kg/mol) and polydispersity of 1.14. To make highly oriented cylindrical P4VP microdomains in a PS matrix, the films were vapor annealed in a saturated toluene/THF (20/80, v/v)

* Corresponding author: E-mail: russell@mail.pse.umass.edu. Telephone: 1-413-545-2680. Fax: 1-413-577-1510.

10.1021/nl0805110 CCC: $40.75
Published on Web 04/30/2008

Scheme 1. Illustration of Gold Decorated Process on Surface Reconstructed Films[a]

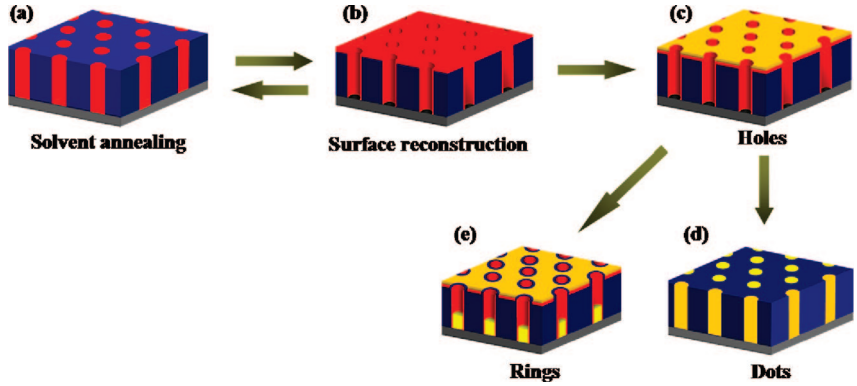

[a] (a) Solvent annealed film. (b) The film reconstructed from ethanol. Solvent annealed and reconstructed films are fully reversible by controlling solvent and temperature. (c) Nanoporous gold film obtained from Au evaporation at a glancing angle. (d) Dots and (e) rings of gold prepared by controlling Au thickness and temperature.

environment for 6 h. Surface reconstruction was achieved by immersing the films in ethanol for 20 min, where ethanol is a good solvent for P4VP but a nonsolvent for PS. To prepare transmission electron microscopy (TEM) samples, the gold decorated PS-*b*-P4VP films were floated off from the silicon substrate in 0.5 wt % HF solution and collected on carbon-coated grids. Bright-field TEM was performed on a (JEOL-1200EX) TEM operating at an accelerating voltage of 100 kV.

Scheme 1 illustrates the process of gold decorated films prepared from nanoporous BCP templates. Highly oriented cylindrical microdomains were developed after solvent annealing in toluene/THF mixed solvent. Nanoporous films were produced by swelling the cylindrical microdomains of the copolymer with a preferential solvent, i.e., ethanol. Because neither block of the copolymer was fundamentally altered by the solvent, the process was fully reversible. By heating the film to near its glass-transition temperature, full recovery of the initial film morphology was achieved. Nanoporous gold film was produced by gold sputtering at a glancing angle (~5°) to the substrate without entering into the pores. By varying the thickness of the gold layer and thermal annealing condition, Au dots and rings were obtained.

Figure 1 shows scanning force microscope (SFM) images of well-developed cylindrical microdomains and the corresponding structure after surface reconstruction. Cylindrical microdomains oriented normal to the substrate, having hexagonal order immediately after spin-coating, have been shown previously.[20] Highly oriented arrays of cylindrical microdomains with ~2 nm depressions were obtained by solvent annealing and are shown in Figure 1a. A reconstructed film having arrays of highly ordered nanopores is shown in Figure 1b. The preferential solvation of P4VP blocks with ethanol is shown to produce a nanoporous template while preserving the order or orientation of the microdomains. Figure 1c shows an SFM image of the film after annealing the reconstructed film at 115 °C for 10 min. It should be noted that the SFM images show that the original structure is retained without any significant change except for changing the film thickness throughout the entire process, where a hexagonal array of cylindrical microdomains or nanopores with an average nearest-neighbor distance of 45.3 ± 2.3 nm and pore diameter of 25.0 ± 1.7 nm. The surface roughness after reconstruction was <0.5 nm.

The reconstructed films are kinetically trapped in an energetically unstable state due to the large surface area produced by the formation of the nanopores and because the surface energy of P4VP is greater than that of PS (γ_{P4VP} = 50.0 mJ/m^2 and γ_{PS} = 45.5 mJ/m^2).[27] Consequently, a recovery to the original morphology would be expected initially by heating the films above the T_g. The thickness of the original and reconstructed films, as measured by optical ellipsometry and X-ray reflectivity, were 24.1 and 27.1 nm, respectively. Upon heating the reconstructed film to 115 °C for 10 min, the thickness decreased to 24.1 nm and the original morphology was recovered (see Supporting Information, Figures S1 and S2). It should be noted that continued heating of the film results in a reorientation of the microdomains parallel to the film surface due to preferential interfacial interactions of P4VP with the substrate and the lower surface energy of the PS block. The movement of P4VP to affect the recovery of the reconstructed films suggests the possibility of using this to control the spatial placement of material placed on the surface of the reconstructed films. Au was thermally evaporated (at a rate of 0.01 nm/s) onto the reconstructed film at a glancing angle under a pressure of 5 × 10^{-6} Torr, to a nominal thickness of 1 nm, as measured by a quartz crystal microbalance. During evaporation, atomic gold diffuses on the surface of the reconstructed film and coalesces, forming nanoparticles. Au preferentially interacts with the P4VP block, and a thin layer (~2 nm on average) of densely pack Au nanoparticles forms on the surface.

Figure 2 shows TEM images of three different reconstructed PS-*b*-P4VP films decorated with Au in different ways, depending on the experimental conditions. Figure 2a shows gold nanoparticles located on top of a reconstructed film, where gold sputtering was carried out at a glancing angle (~5°) to the substrate so that gold nanoparticles selectively decorated the film surface only, without entering into the pores. Consequently, a nanoporous gold film is produced that is suitable as a mask for pattern transfer. By heating an Au-decorated reconstructed film, having a gold

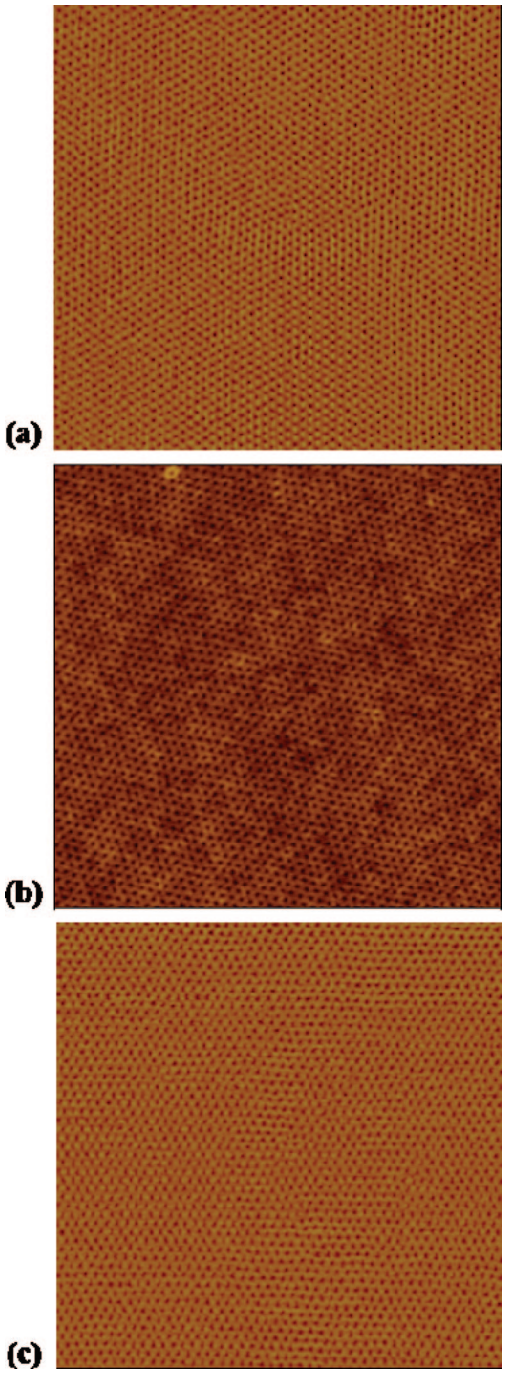

Figure 1. SFM images of well-developed PS-*b*-P4VP hexagonal structures (2 μm $\times$ 2 μm in height mode). (a) Film is annealed in toluene/THF solvent mixture. (b) Film is surface reconstructed in ethanol. (c) Recovery to initial morphology after heat treatment.

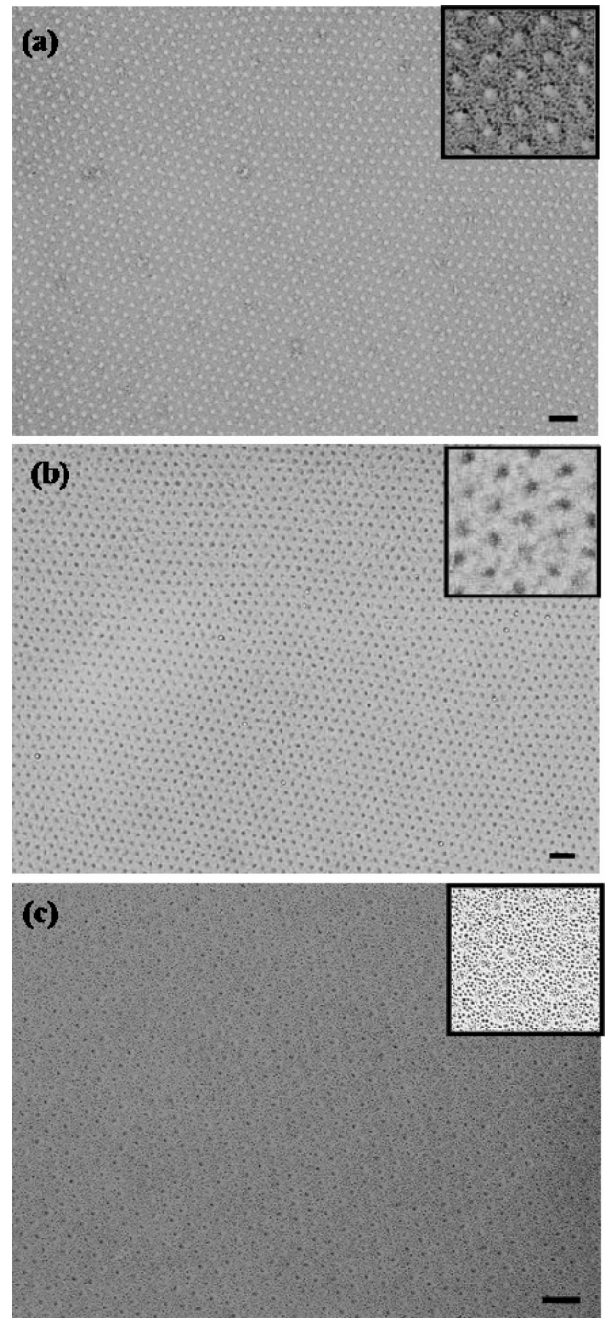

Figure 2. Gold decoration on the reconstructed PS-*b*-P4VP films (a) outside the pore, (b) inside the pore, and (c) having the ring pattern. Three magnified images are shown in the inset indicating the gold nanoparticles (scale bar: 100 nm).

layer thinner than ~0.5 nm, to 115 $\pm$ 1 °C for 10 min, the Au nanoparticles are drawn into the pore along with the P4VP, as shown in Figure 2b. If the gold layer is thicker than 0.5 nm, this does not occur. It should be noted that even after the gold goes into the pore, the size of cylindrical microdomains does not change in comparison to that of the reconstructed film. When the annealing temperature is increased to 180 °C for 30 min, the gold-coated reconstructed films undergo a different recovery. If the thickness of the evaporated gold is >0.5 nm, some of the Au is drawn into the pores, forming nanoparticles in the center of the microdomain, leaving the remainder on the surface. Viewed from above, a ring pattern forms, as shown in Figure 2c. This pattern is also suitable for transfer to the underlying substrate. In addition, this process offers a simple but direct means of placing nanoparticles at a precise location between two conducting or semiconducting layers.

To investigate the preferential interaction of Au with P4VP, morphologies obtained after deposition of thin Au layers onto PS and P4VP (number-average molecular weight, M_n^{PS} = 33 kg/mol, M_w/M_n = 1.04, and M_n^{P4VP} = 46.7 kg/

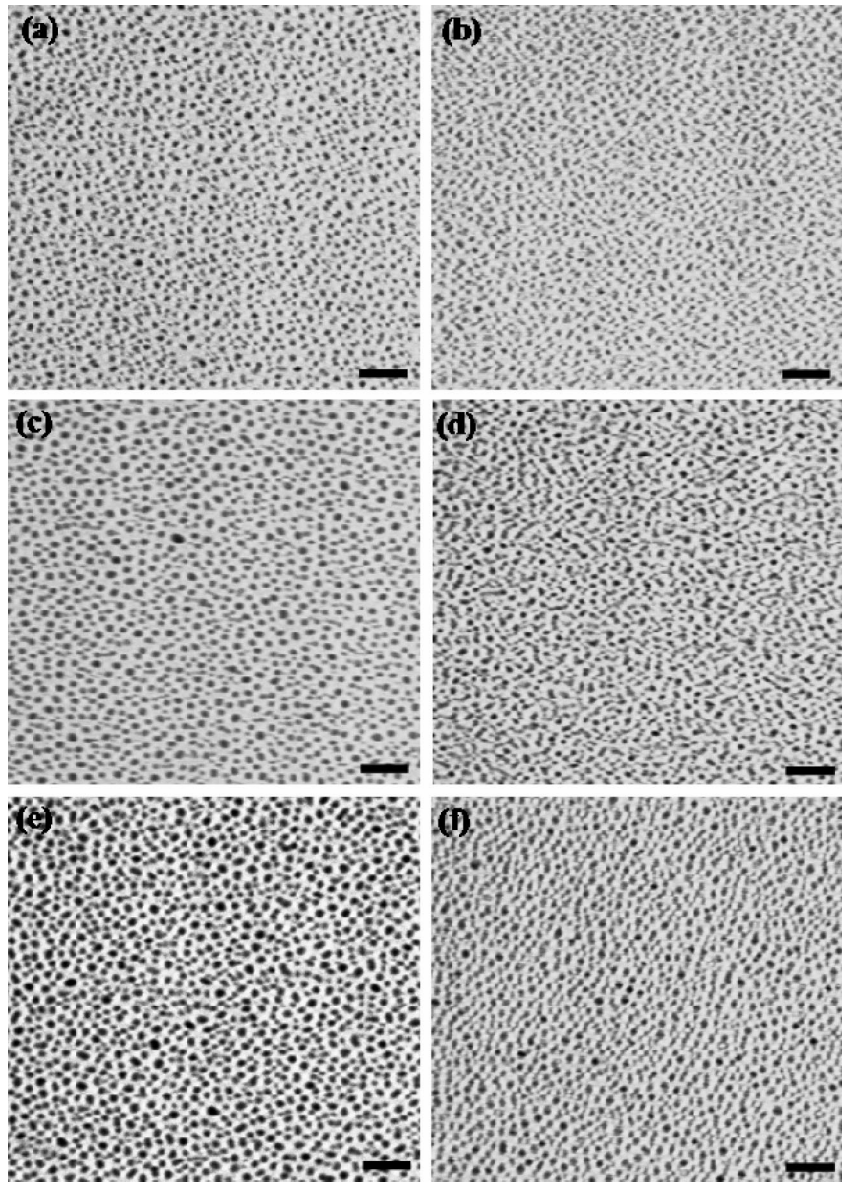

Figure 3. TEM images of 1 nm thick Au layers deposited onto PS (a,c,e) and P4VP (b,d,f) matrices. (a,b) As-evaporated, (c,d) thermal annealing at 115 °C for 10 min, and (e,f) thermal annealing at 180 °C for 30 min (scale bar: 50 nm).

mol, $M_w/M_n = 1.14$, Polymer Source) matrices were examined by TEM before and after thermal annealing, as shown in Figure 3. Au layers with an average thickness of ~1 nm were deposited onto thin films of PS and P4VP. Initially deposited Au layers exist as isolated islands because the Au does not wet the polymer matrices. The size of Au deposited on PS is larger when compared to those on P4VP due to the preferential interactions of P4VP with Au, as shown in Figure 3a,b. After thermal annealing, the morphologies of the Au layers deposited onto PS and P4VP homopolymer are different. When the polymer films are annealed at 115 °C for 10 min, the Au particles on PS get larger than on P4VP, where the interactions of P4VP with Au reduce the mobility of the Au (Figure 3c,d). This behavior is exacerbated at elevated temperature. Figure 3e,f shows a TEM image of Au layers that were annealed at 180 °C for 30 min. The size of the Au deposited onto PS at elevated temperatures increases due to the increased mobility of the Au nanoparticles. On P4VP, though, the size of the Au particles does not change (see Supporting Information, Figure S3). The high binding energy of a gold atom to an individual gold nanoparticle ensures that island growth occurs by the motion and coalescence of individual islands.[28]

Gold was also evaporated onto the solvent annealed films without the pores at a glancing angle. As shown in Figure S4a, Supporting Information, gold was located everywhere on the film right after the evaporation. After annealing the films at 110 °C for 10 min or 180 °C for 30 min, no selective gold decoration was observed (see Supporting Information, Figure S4). Instead, gold nanoparticles were not only aggregated on PS matrix but also partially located at P4VP blocks, indicating that the surface reconstructed film plays a key role in controlling the spatial location of gold nanoparticles.

The location of gold nanoparticles on the PS-*b*-P4VP film was also investigated by grazing incidence small-angle X-ray

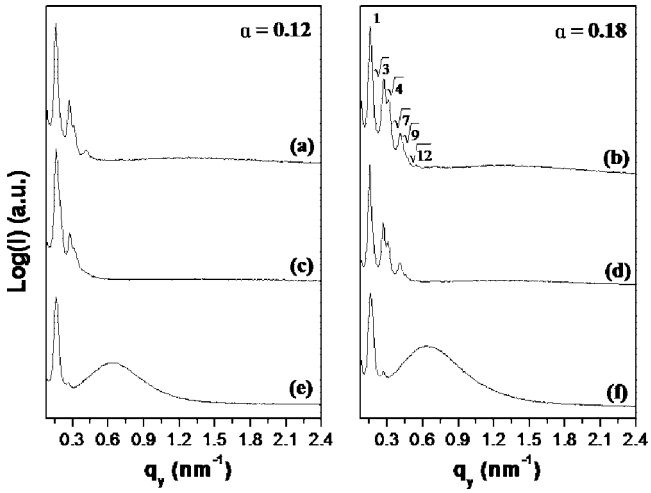

Figure 4. GISAXS patterns of three different gold decorated PS-*b*-P4VP films. (a,b) Top of reconstructed films, (c,d) inside P4VP cylindrical domains, and (e,f) top of films and inside P4VP cylinder.

scattering (GISAXS). GISAXS measurements were performed at beamline X22B (National Synchrotron Light Source, Brookhaven National Laboratory) using X-rays with a wavelength of $\lambda = 1.525$ Å. The GISAXS patterns were measured below ($\alpha = 0.12°$) and above ($\alpha = 0.18°$) the critical angle of the polymer ($\alpha_c = 0.16°$). The former provides structural information at the surface, while the latter provides structural information throughout the film. GISAXS patterns for the reconstructed film coated with Au under different annealing conditions are shown in the Supporting Information (see Supporting Information, Figure S5). A cursory examination of these profiles is that the interferences characteristics of the hexagonal array of the microdomains are extended in the q_z direction, i.e., normal to the film surface. Further assessment of the scattering requires a closer examination of the profiles. Shown in Figure 4a−f are traces taken along the horizon, i.e., along q_y ($q_z = 0$). For the reconstructed film with Au evaporated on the surface, the GISAXS profiles above and below the critical angle are identical in shape, although the intensities differ. For $\alpha < \alpha_c$, scattering characteristic of a hexagonal array of holes in the Au film is seen. For $\alpha > \alpha_c$, a significant increase in the scattering is seen due to an increase in the contrast, i.e., the electron density difference between the air in the pores and the matrix. Hence, an increase in the intensity and a sharpening of the interference maxima in the GISAXS, for $\alpha > \alpha_c$, are seen in Figure 4a,b. As shown in the TEM image in Figure 2b, the GISAXS results indicate that Au is uniformly distributed in the cylindrical microdomains as one proceeds from the top of the film to the bottom, as shown in Figure 4c,d. The Au has been drawn into the cylindrical microdomains, but there does not appear to be any significant aggregation of the Au in the pores as indicated in Figure 3. Now, when the thickness of the Au is >0.5 nm, the scattering arising from the gold layer is seen for $\alpha < \alpha_c$ and $\alpha > \alpha_c$ (Figure 4e,f). However, a pronounced maximum arising from the form factor of Au nanoparticles within the pore is seen. This scattering is not seen in the other cases, indicating that

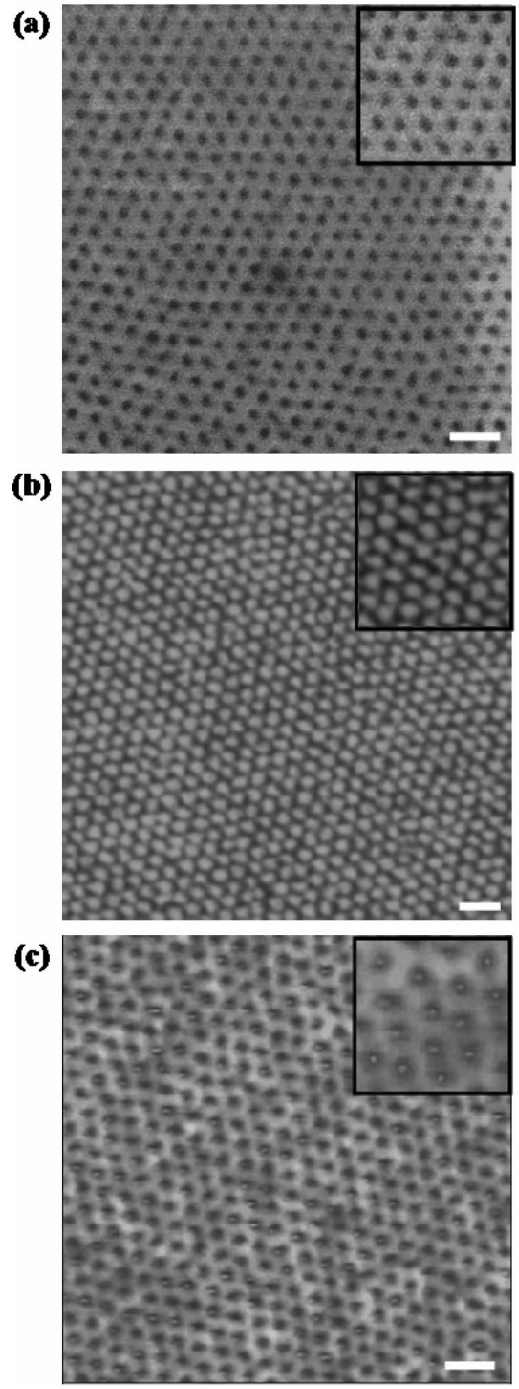

Figure 5. Pattern transfer of gold decorated PS-*b*-P4VP templates into silicon oxide. SEM images of nanostructures with nanosized pore (a), pillar (b), and ring pattern (c) on silicon were shown after RIE etching. Three magnified images are shown in the inset indicating the gold nanoparticles and pattern transfer (scale bar: 100 nm).

the formation of Au nanoparticles does not occur. It should be noted that scattering from the nanodots is characteristic of a single layer at the substrate interface.

To transfer the pattern produced by the gold coated polymer films into the underlying substrate, the films were exposed to a SF_6 RIE [TRION technology, at 50 mTorr pressure, 25 SCCM (SCCM denotes standard cubic centimeter per minute) flow rate, and 40 W power]. After etching

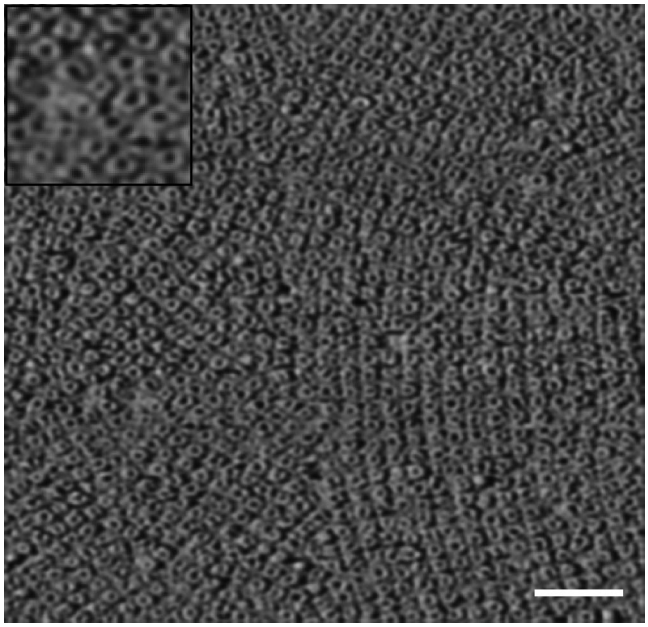

Figure 6. SEM image of Cr ring pattern prepared from template having gold decorated ring pattern. In the inset, the Cr ring pattern was clearly seen (scale bar: 200 nm).

into the silicon oxide, the gold coated films were removed with a 10 wt % KI/I_2 (4/1, v/v) solution, followed by oxygen plasma etching for 10 min. Figure 5 shows pattern transfer of three gold decorated polymer templates into silicon oxide using SF_6 RIE, which are identical to that seen in the original template. In the inset, pattern transfer results are magnified for clarity. It should be noted that the metal coated films can be used as hard etching masks for pattern transfer into the underlying substrate.

In addition to pattern transfer from gold decorated films, a chromium (Cr) nanoring pattern could also be produced. Figure 6 shows the SEM image of a Cr nanoring pattern obtained from the gold decorated films having ring pattern. The gold decorated nanoring pattern was reactively ion etched (TRION technology, at 50 mTorr pressure, 30 SCCM flow rate, and 50 W power) with CHF_3 to remove polymer surrounding the Au nanoparticles in the cylindrical microdomains. Then, Cr was thermally evaporated onto the etched template to a nominal thickness of ~8 nm, as measured by a quartz crystal microbalance. The films were then sonicated in chloroform for 5 min to remove the excess Cr. In the inset of the top left corner, the magnified Cr ring pattern was clearly seen with a long-range order.

In summary, we have demonstrated three approaches for the incorporation of gold into nanopatterned PS-*b*-P4VP films. Films of PS-*b*-P4VP having arrays of highly ordered P4VP cylindrical microdomains were prepared by solvent annealing. Using a preferential solvent for P4VP, a reversible reconstruction of the films occurred, producing a nanoporous template. By varying the amount of Au evaporated onto the surface, the nanoporous films could be produced and annealed to draw the Au into the cylindrical microdomains or a nanoporous Au film with Au nanodots at the base of the pores could be produced. The gold coated polymer templates could be transferred into silicon oxide with high fidelity using RIE and Cr ring pattern could be obtained from a gold decorated template.

Acknowledgment. This work was supported by the U.S. Department of Energy (DOE), the NSF supported MRSEC and NSEC at the University of Massachusetts Amherst. Use of the National Synchrotron Light Source, Brookhaven National Laboratory, was supported by the U.S. Department of Energy, Office of Science, Office of Basic Energy Sciences, under contract no. DE-AC02-98CH10886.

Supporting Information Available: Polymer thickness, Size distribution of Au particles, and GISAXS results. This material is available free of charge via the Internet at http://pubs.acs.org.

References

(1) Jaramillo, T. F.; Baeck, S. H.; Cuenya, B. R.; McFarland, E. W. *J. Am. Chem. Soc.* **2003**, *125*, 7148.
(2) Feldheim, D. L.; Grabar, K. C.; Natan, M. J.; Mallouk, T. E. *J. Am. Chem. Soc.* **1996**, *118*, 7640.
(3) Honda, K.; Rao, T. N.; Tryk, D. A.; Fujishima, A.; Watanabe, M.; Yasui, K.; Masuda, H. *J. Electrochem. Soc.* **2001**, *148*, A668.
(4) Bockstaller, M. R.; Mickiewicz, R. A.; Thomas, E. L. *Adv. Mater.* **2005**, *17*, 1331.
(5) Fan, H. J.; Werner, P.; Zacharias, M. *Small* **2006**, *2*, 700.
(6) Haryono, A.; Binder, W. H. *Small* **2006**, *2*, 600.
(7) Black, C. T.; Murray, C. B.; Sandstrom, R. L.; Sun, S. *Science* **2000**, *290*, 1131.
(8) Thurn-Albrecht, T.; Schotter, J.; Kästle, G. A.; Emley, N.; Shibauchi, T.; Krusin-Elbaum, L.; Guarini, K.; Black, C. T.; Tuominen, M. T.; Russell, T. P. *Science* **2000**, *290*, 2126.
(9) Lopes, W. A.; Jaeger, H. M. *Nature* **2001**, *414*, 735.
(10) Cheng, G.; Moskovits, M. *Adv. Mater.* **2002**, *14*, 1567.
(11) Gorzolnik, B.; Mela, P.; Moeller, M. *Nanotechnology* **2006**, *17*, 5027.
(12) Sohn, B.-H.; Choi, J.-M.; Yoo, S. I.; Yun, S.-H.; Zin, W.-C.; Jung, J. C.; Kanehara, M.; Hirata, T.; Teranishi, T. *J. Am. Chem. Soc.* **2003**, *125*, 6368.
(13) Thompson, R. B.; Ginzburg, V. V.; Matsen, M. W.; Balazs, A. C. *Science* **2001**, *292*, 2469.
(14) Hamley, I. W. *Angew. Chem., Int. Ed.* **2003**, *42*, 1692.
(15) Chiu, J. J.; Kim, B. J.; Kramer, E. J.; Pine, D. J. *J. Am. Chem. Soc.* **2005**, *127*, 5036.
(16) Kim, B. J.; Chiu, J. J.; Yi, G.; Pine, D. J.; Kramer, E. J. *Adv. Mater.* **2005**, *17*, 2618.
(17) Lin, Y.; Böker, A.; He, J.; Sill, K.; Xiang, H.; Abetz, C.; Li, X.; Wang, J.; Emrick, T.; Long, S.; Wang, Q.; Balazs, A.; Russell, T. P. *Nature* **2005**, *434*, 55.
(18) Ansari, I. A.; Hamley, I. W. *J. Mater. Chem.* **2003**, *13*, 2412.
(19) Xu, T.; Stevens, J.; Villa, J.; Goldbach, J. T.; Guarini, K. W.; Black, C. T.; Hawker, C. J.; Russell, T. P. *Adv. Funct. Mater.* **2003**, *13*, 698.
(20) Park, S.; Wang, J.-Y.; Kim, B.; Chen, W.; Russell, T. P. *Macromolecules* **2007**, *40*, 9059.
(21) Park, S.; Kim, B.; Wang, J.-Y.; Russell, T. P. *Adv. Mater.* **2008**, *20*, 681.
(22) Park, M.; Chaikin, P. M.; Register, R. A.; Adamson, D. H. *Appl. Phys. Lett.* **2001**, *79*, 257.
(23) Cheng, J. Y.; Ross, C. A.; Thomas, E. L.; Smith, H. I.; Vancso, G. J. *Appl. Phys. Lett.* **2002**, *81*, 3657.
(24) Meli, M.-V.; Badia, A.; Grütter, P.; Lennox, R. B. *Nano. Lett.* **2002**, *2*, 131.
(25) Guarini, K. W.; Black, C. T.; Zhang, Y.; Kim, H.; Sikorski, E. M.; Babich, I. V. *J. Vac. Sci. Technol., B* **2002**, *20*, 2788.
(26) Kubo, T.; Parker, J. S.; Hillmyer, M. A.; Leighton, C. *Appl. Phys. Lett.* **2007**, *90*, 233113.
(27) Sohn, B.-H.; Seo, B.-W.; Yoo, S. I.; Zin, W.-C. *Langmuir* **2002**, *18*, 10505.
(28) Kunz, M. S.; Shull, K. R.; Kellock, A. J. *J. Appl. Phys.* **1992**, *72*, 4458.

NL0805110